Cardiovasc Intervent Radiol (2018) 41:1428–1435
https://doi.org/10.1007/s00270-018-2001-5

TECHNICAL NOTE

Evaluation of the Needle Positioning Accuracy of a Light Puncture Robot Under MRI Guidance: Results of a Clinical Trial on Healthy Volunteers

Julien Ghelfi[1] · Alexandre Moreau-Gaudry[2,3,4,5] · Nikolai Hungr[6] · Céline Fouard[6] · Baptiste Véron[6] · Maud Medici[4,7,8] · Emilie Chipon[4,7,8] · Philippe Cinquin[6] · Ivan Bricault[1]

Received: 8 December 2017 / Accepted: 26 May 2018 / Published online: 6 June 2018

Abstract
Purpose To assess the accuracy of Light Puncture Robot (LPR) as a patient-mounted robot, in positioning a sham needle under MRI guidance for abdominal percutaneous interventions.
Materials and Methods This monocentric, prospective and non-controlled study was approved by the ethics review board. The study evaluated the accuracy of LPR V3 to achieve a virtual puncture in 20 healthy volunteers. Three trajectories were tried on each volunteer, under 3-T MRI guidance.
Results Accuracy under 5 mm in attaining a 10 cm-deep target was reached in 72% of attempts after 2 robot motions with a median error of 4.1 mm [2.1; 5.1]. Median procedure time for one trajectory was 12.9 min [10.2; 18.0] and median installation time was 9.0 min [6.0; 13.0].
Conclusion LPR accuracy in the deployment of a sham needle inside the MRI tunnel and its setup time are promising. Further studies need to be conducted to confirm these results before clinical trials.

Keywords Percutaneous interventions · MRI guidance · Robot

✉ Julien Ghelfi
JGhelfi@chu-grenoble.fr

Alexandre Moreau-Gaudry
Amoreau-gaudry@chu-grenoble.fr

Nikolai Hungr
nikolaiahungr@hotmail.com

Céline Fouard
Celine.fouard@univ-grenoble-alpes.fr

Baptiste Véron
Baptiste.veron@univ-grenoble-alpes.fr

Maud Medici
mmedici@chu-grenobe.fr

Emilie Chipon
echipon@chu-grenoble.fr

Philippe Cinquin
Philippe.cinquin@univ-grenoble-alpes.fr

Ivan Bricault
IBricault@chu-grenoble.fr

[1] Clinique Universitaire de Radiologie et Imagerie Médicale, CHU de Grenoble, BP 217, 38043 Grenoble Cedex 09, France

[2] TIMC-IMAG, Univ. Grenoble-Alpes, 38000 Grenoble, France

[3] TIMC-IMAG, CNRS, 38000 Grenoble, France

[4] Inserm CIC 1406, 38000 Grenoble, France

[5] Pole Sante Publique, CHU Grenoble-Alpes, 38000 Grenoble, France

[6] Laboratoire TIMC-IMAG (UMR CNRS 5525) - Équipe GMCAO, Faculté de Médecine - Pavillon Taillefer, 38706 La Tronche Cedex, France

[7] CIC 1406, Univ. Grenoble-Alpes, 38000 Grenoble, France

[8] Pole Recherche, CHU Grenoble-Alpes, 38000 Grenoble, France

Introduction

Percutaneous image-guided interventions are increasing in number in clinical practice because they are minimally invasive [1]. Needle placement is crucial and highly dependent on the physician's skills and experience with a freehand technique. It is often the longest part of the intervention [2]. Challenging targets, requiring double-oblique trajectories, can lead to placement errors and consequently multiple needle adjustments. This may be responsible for the duration of long procedures, greater exposure of the patient to radiation (under CT scan) and injury to nearby organs or vessels [3].

For these reasons, assisted systems have been developed to improve needle placement [4]. They may help the radiologist to achieve complex needle trajectories, increase precision and tend to offer faster and safer procedures [5, 6]. The accuracy of various table-mounted robots has been well studied [7–11]. Two patient-mounted robots [12, 13] have also been developed, with accuracy reported as compatible with clinical practice, but these robots are not MRI compatible. In addition, Wu et al. [14] have developed a small needle manipulator mounted on an MRI loop coil to perform rapid guidance.

The Light Puncture Robot (LPR) (Fig. 1) is a new multimodal patient-mounted interventional radiology robot for percutaneous needle interventions [15]. This compact robot (368 mm × 270 mm × 127 mm) is entirely made of non-magnetic materials (primarily polycarbonate and carbon fiber) to be fully compatible with both CT and MR imaging. The robot is strapped to the patient's body allowing it to move with the patient without jeopardizing his safety or the integrity of the insertion. Two previous prototypes have already been developed and described in previous publications [16–19].

The purpose of this study is to evaluate the accuracy of LPRV3 in its first clinical tests performed on healthy volunteers under MRI guidance using a virtual needle.

Materials and Methods

Study Design

This prospective single-arm pilot study was conducted at a single center to evaluate the accuracy of LPR in a population of 20 healthy volunteers. The study protocol was approved by our institutional ethics review board and by the French National Medical Safety Authority. Written informed consent was obtained from all volunteers. Our study was registered on the Clinical Trials Registry (Number NCT02360241). The prototype passed all conducted disturbances, radiated electric field, harmonic current emissions and voltage fluctuation and flicker measurements for a class A device according to the European EN 60601-1-2 standards.

Eligibility

Volunteers were adults who could stay in the MRI bore with the robot placed on their abdomen. Inclusion criteria were adult aged 18 years or more, height inferior to 1m90, maximum abdominal thickness less than 28 cm, abdominal width between 26 and 50 cm, maximum abdominal perimeter of 125 cm and a capacity to hold their breath for 30 s. Exclusion criteria were claustrophobia, pregnancy and standard MRI contraindications.

LPR V3 Prototype

LPR V3 is based on a parallelogram design that gives the robot two translational degrees of freedom (DOF) and two rotational DOF (Fig. 1). The two parallel platforms are translated by four Shinsei USR60-E3N piezoelectric motors (Shinsei Corp., Tokyo, Japan). Because motors interfered with the MRI image when powered inside the tunnel, they are set at the volunteer's feet, in a container located on the MRI bed.

The control electronics are housed in a separate control box that can be placed outside the imaging room to prevent it from affecting the image quality, during MRI guidance.

The needle is held by two independent grippers (Fig. 1), the lower one being stationary and the top being mobile in the direction of the needle's axis. By releasing the lower grip and activating the upper grip, the needle can be inserted or withdrawn by moving the upper grip up or down. These motions are actuated using pneumatic solenoid valves connected to the hospital's medical air supply. The insertion stroke depth is controlled using a fifth piezoelectric motor and Bowden cable combination that sets a stopper depth using a series of gears and a screw. Using two grippers ensures that the needle is gripped throughout its insertion and the needle grips are powered by bi-directional pneumatic valves, allowing them to completely release the needle.

To prevent any contamination, the robot frame remains within the constraints of the hydrogen peroxide STERRAD sterilization machine. The fixation module consists of a thin fixation frame to which the robot can be clipped by aligning four pegs and pushing the robot frame down onto them (Fig. 2). A sterile drape can be inserted between the robot module and the fixation frame, making it unnecessary to sterilize the fixation module. A standard 62 × 38 cm rectangular VacFix® radiology vacuum cushion (Qualimedis, Maisons-Alfort, France) used to stabilize patients

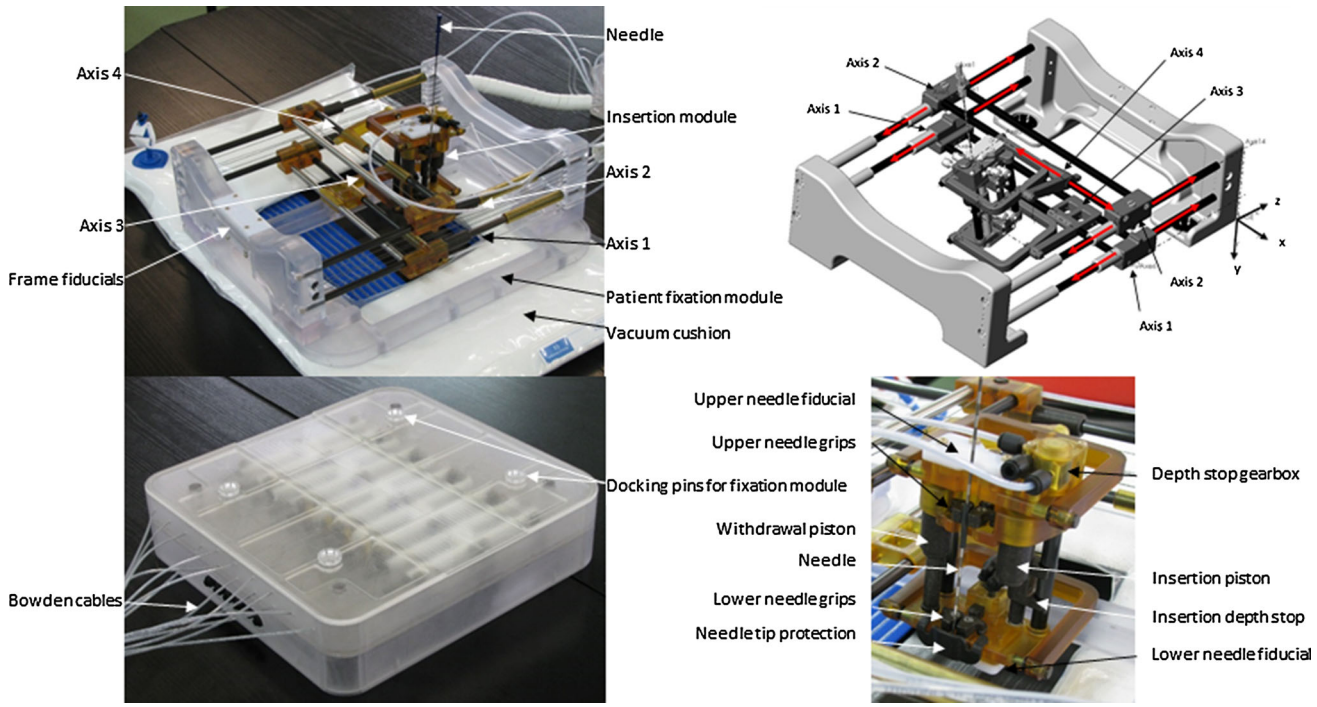

Fig. 1 Clinical prototype of the LPR V3 robot. Top-left: the robot module mounted onto the fixation module. Top-right: CAD Model of the LPR V3 prototype showing the four primary axes of motion. Axes 1 and 2 are pulled by cables at two locations each, while axes 3 and 4 are only pulled at one location each. Bottom-left: motor box used to pull the Bowden cables. Bottom-right: detail of insertion module showing the needle grips, insertion pistons and depth stop mechanism

during intervention is placed between the patient's skin and the fixation frame.

The robot is detected in the CT and MR images using fiducials embedded into the robot module's structure [17]. Two distinct fiducials are placed on the upper and lower parallel platforms as close to the needle axis as possible. On this new prototype, two additional fiducials were incorporated in the robot module's frame to provide secondary backup detection (Fig. 3).

Procedure

Each volunteer was placed in a supine position in a 3T Achieva® MRI bore (Philips, Amsterdam, Netherlands). Four 6 mm diameter MRI-visible markers (MR-Pinpoint Small Field View, Beekley Corporation, Bristol, CN) were fixed on the volunteer's skin, one on the back as a "target" and three on the abdomen as "skin entry points," (Fig. 4). This configuration allowed the radiologist to plan three trajectories with the robot in various poses.

The LPR prototype was strapped on the volunteer's abdomen above the rectangular vacuum cushion with a sterile drape (Fig. 5). As no coil could be set on the robot, volume coils directly integrated into the MR bore were used. Motors were set at the volunteer's feet and connected to the control computer in the operator's room. A hermetic glass needle filled with gadolinium contrast agent Marcol 82 (Philips, Amsterdam, Netherlands) was used [20].

The MRI sequence was a T1-weighted High Resolution Isotropic Volume Examination sequence (e-THRIVE: TR = 2.88 ms, TE = 1.32 ms, flip angle = 10°), with 2-mm axial slice-spacing and 0.488 mm reconstruction pixel size for each slice. A first sequence was acquired to identify cutaneous MRI-visible markers and fiducials in the field of view (FOV). Then, images were transferred to the control computer as DICOM fields. For this protocol, specific software was developed using the CamiTK framework [21]. After automatic registration of the robot (via automatic segmentation of the robot's fiducials), the software was used for path planning (Fig. 4). The interventional radiologist selected a target (the cutaneous marker located on the volunteer's back), a skin entry point (one of the 3 markers located on his abdomen) and validated the proposed robot motion. The robot then aligned the needle with the planned trajectory and a second identical image was taken to control the needle position. For this, the fiducials and two skin markers were once again segmented to superimpose the planned trajectory on the current virtual needle position defined by the segmentation. A cylinder was then calculated, centred on the planned trajectory, that encompassed the current virtual needle trajectory between the target and the entry points. The radius of this cylinder

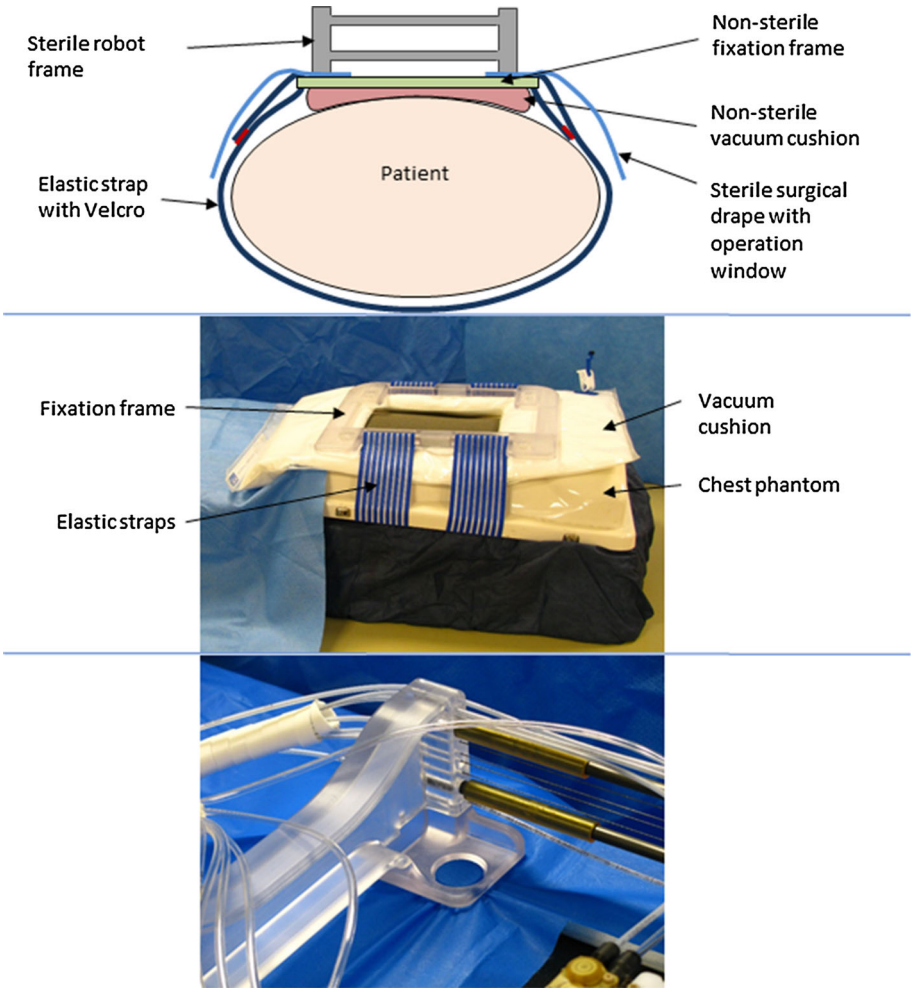

Fig. 2 Top: Image showing the concept of the fixation module for holding the robot to the patient's body. Middle: Image showing the various components of the fixation module mounted on a chest phantom. Bottom: Image showing the robot module clipped onto the fixation frame through a sterile drape

was used as the accuracy with which the robot had aligned the needle with the planned trajectory. If this error was greater than 5 mm, the robot could move the needle closer if possible, after which a new control image was taken. No more motions were allowed for this protocol. Once finished, the robot was repositioned in its home position. This procedure was repeated for each cutaneous entry mark (Fig. 5). There was no actual needle insertion in this pilot study with volunteers and the motor effecting insertion had been deactivated.

Outcomes

The primary aim was to evaluate the accuracy of the fictitious needle positioning in comparison to the planned path, to attain a 10 cm-deep target (Fig. 6). This standard depth was fixed to achieve reliable measurements. Two attempts were allowed to reach an accuracy of within 5 mm of the planned trajectory that is the radius of the minimum size of lesion likely to be targeted using CT or MRI.

Secondary aims included procedure duration, robot detection robustness and volunteer discomfort. To quantify robot detection robustness, we recorded the number of times fully automatic segmentation failed, requiring the radiologist to pass to the semi-automatic mode. Each segmentation result was qualitatively verified and validated by the radiologist during the procedure using a display of a model of the fiducials directly on the image. At the end of the procedure, the volunteer rated the discomfort caused by the robot on a scale of 0–3 (0 being very comfortable and 3 being very uncomfortable).

Statistical Analysis

In this pilot study, descriptive statistical tools were used. The normality of the quantitative parameters was determined by the Shapiro–Wilks test. Parameters with normal distribution are presented as the mean and standard deviation. Otherwise the median, with 25th and 75th percentiles, is given. Qualitative parameters are expressed as number and percentage.

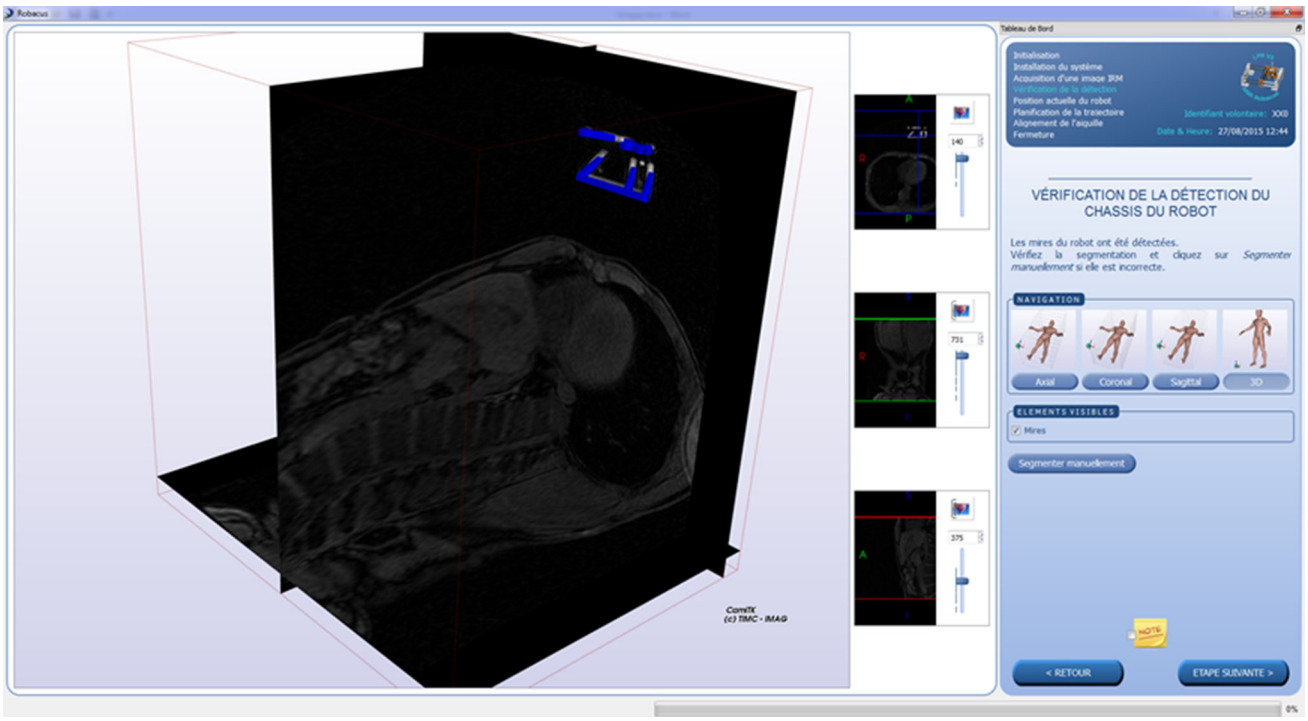

Fig. 3 Screenshot showing the "robot frame" fiducial displayed over a 3D representation of the MR image. This screen was used by the radiologist to verify the fiducial segmentation

Results

20 healthy volunteers were included during March 2015 and 3 different trajectories were planned in each volunteer (Table 1).

Among the 60 trajectories planned, two were cancelled because the cutaneous markers were not located in the robot's workspace. Concerning the 58 trajectories achieved, an accuracy within 5 mm was reached in 42 of the planned trajectories (72%) with 2 motions or less (Table 2). Median accuracy to position the fictitious needle over a 10 cm-deep target was 4.1 mm [2.1; 5.1]. No relationship between the robot's accuracy and patients' BMI or abdominal perimeter was found.

Median procedure time for one trajectory was 12.9 min [10.2; 18.0]. The median installation time was 9.0 min [6.0; 13.0].

91% of the frame fiducial segmentations and 76% of the needle fiducial segmentations could find a complete solution fully automatically, the rest requiring input from the radiologist using the semi-automatic routine.

None of the volunteers ranked the robot as the first cause of discomfort during the procedure. Two volunteers reported slight discomfort in breathing owing to the robot's frame (rated 1/3 on the scale). The main cause of discomfort during the procedure was due to apnea (55%).

Discussion

The experiments showed promising results concerning the feasibility of the system for assisting radiologists in reaching complex targets with double-oblique trajectories. Median accuracy to reach a 10 cm depth target was 4.1 mm over a wide variety of body sizes and anatomies. These results are encouraging given the errors inherent to such an image-guided technique, in particular the motion of the patient due to the breath, the relatively low image resolution and the constraints of MRI image and material compatibility.

In recent years, many robotic systems have been developed, but only a few are used in clinical practice. Commercially available robots are mainly table-mounted systems. The accuracy of the LPR had already been validated on phantoms [16]. This was the first evaluation of the LPR prototype performed in an MRI facility with healthy volunteers. The MRI setting induces technical and material constraints related to magnetic field and to the limited access to the patient inside the tunnel. To deal with these technical obstacles, some authors propose to use robots to position the needle and then to insert it manually [10]. Concerning patient access constraints, some authors suggest performing needle insertion outside of the tunnel, as could be done using the majority of table-mounted robots. However, there would remain problems related to patients

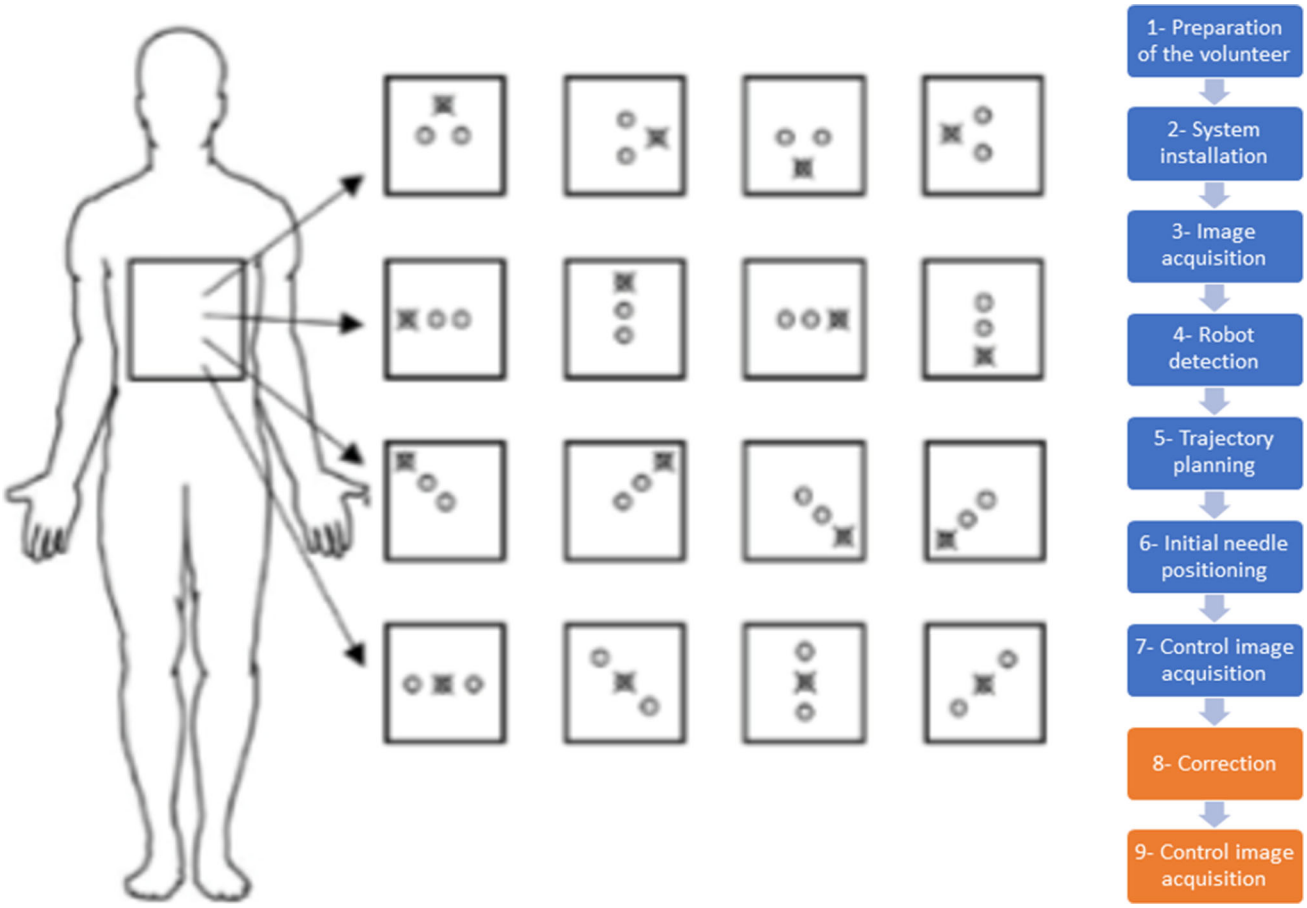

Fig. 4 Planning of the procedure. Distribution of the trajectories planned on each patient. The square represents the robot's workspace. Each square represents the robot's workspace, within which three different skin entry points (circles) on the subject's front were used to orient the needle towards a single target (cross) on the patient's back. On the right, steps of the clinical protocol used during the human trial

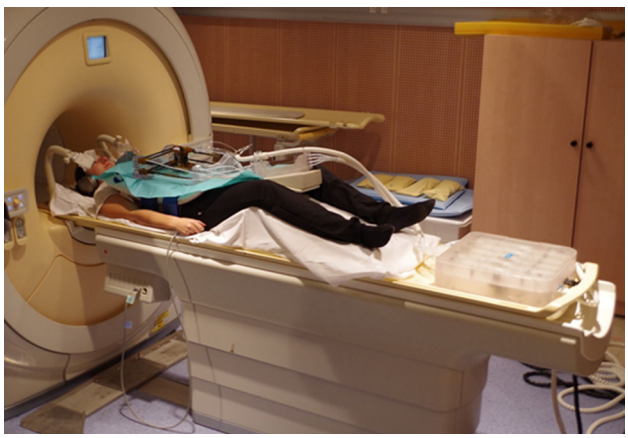

Fig. 5 The LPR V3 system installed on a volunteer in the MRI. The robot is on the subject's torso and the motor box is at the subject's feet on the MRI table

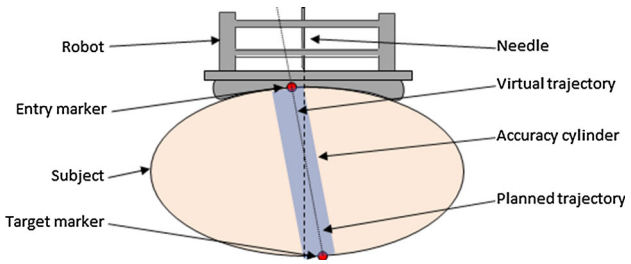

Fig. 6 Schematic showing how the robot accuracy was determined in the control images using the planned and virtual needle trajectories. The target and entry markers are represented as circles. The planned trajectory spanning these two markers is represented as a dotted line. The virtual trajectory of the current needle's position is represented as a dashed line. A cylinder parallel to the planned trajectory is determined, containing exactly both the planned and virtual trajectories between the two markers

shifting position during long and uncomfortable procedures. Moreover, this type of needle insertion does not allow real-time images to be collected during insertion [10].

Contrary to most of robotic systems, LPR compatibility with both CT and MRI is a major advantage. Indeed, these two imaging modalities do not compete but can provide complementary information. Some procedures require data about soft tissues that are only available under MRI, while

Table 1 Description of the study population ($N = 20$)

Characteristics	Patients ($N = 20$)
Age (years)	28 [26; 30][a]
Male *N* (%)	11 (55)
Female *n* (%)	9 (45)
Weight (kg)	68.5 (13.8)[b]
Height (cm)	174 (8, 0)[b]
BMI	22.5 (3, 0)[b]
Abdominal perimeter (cm)	85 (8, 3)[b]
Thoracic perimeter (cm)	93 (7.1)[b]

[a]Median (interquartile range)

[b]Average (standard deviation)

Table 2 Results of LPR clinical trial

Robot accuracy	*N* (%)
Success after 1 motion	17 (29)
Success after 2 motions	25 (43)
More than 5 mm after 2 motions	16 (28)
Duration (min)	Median [Q1; Q3]
Installation time	9 [6, 13]
Procedure time	12.9 [10.2; 18.0]
Dismantling time	2 [1; 2]
Frame fiducial segmentation	*N* (%)
Automatic	53 (91)
Semi-automatic	5 (9)
Needle fiducial segmentation	*N* (%)
Automatic	44 (76)
Semi-automatic	14 (24)
Main cause of discomfort	*N* (%)
LPR prototype	0 (0)
Holding breath	11 (55)
Staying in MRI tunnel	4 (20)
Remaining supine	3 (15)
MR instrument noise	1 (5)
None	1 (5)

others can be performed under CT scan guidance. The use of a multimodal robotic system may also be an advantage to promote learning and improve the standardization of procedures.

To achieve reliable measurements, we had to definite a standard depth for the procedure. Based on the hypothesis that most targets reached on percutaneous procedures are located under 10 cm of the entry point, we chose this measurement. The minimum size of lesion likely to be targeted using CT or MRI is about 5 mm in radius. Smaller lesions can be difficult to locate in the images and are often not considered clinically serious enough to warrant invasive diagnosis or treatment. We, therefore, chose a desired accuracy of less than 5 mm, which would allow lesions with at least a 10 mm diameter to be successfully targeted. Despite most of the commercial available MRI-compatible biopsy devices are eligible only for 1.5T, we chose a 3T MRI for our protocol as our academic center had a 3T MRI dedicated for research. We use 3D T1-weighted sequence to allow good recognition of fiducials. As we did not reach anatomical targets, using a T2 sequence that allows a better visualization of anatomic structure was not necessary. Future trials on patients will be planned on T2 sequences.

Timewise, the system was very reasonable, with short installation time and consistently rapid dismantling time. All subjects were surprised how they hardly noticed the robot's weight on their abdomen and chest, even when the radiologist had to exert pressure on the robot's frame to clip it onto the fixation frame. No subjects complained of having their breathing significantly restricted, which was particularly important due to the relatively long and numerous breath-holds required of them. The main sources of discomfort were the 28-second-long apneas, and the tight MRI tunnel.

The major limitation of this study is the use of a mock needle with no real needle insertion. Clinical development of the prototype required us to first assess the robot's compatibility with use in an MRI tunnel on healthy volunteers before performing real needle insertion. However, the clinical pertinence can only be evaluated after full needle insertion tests are done, considering the needle tissue and deflection issues.

The inaccuracies of the system come from a number of sources. The robot's intrinsic accuracy is dependent on the calibration of the robot's Dyneema cables. As described previously [19], stretch of the cables creates large discrepancies between the commanded motor position and the actual position actuated at the other end of the cables. The effectiveness of the calibration method was evaluated by repeating the calibration 9 times to see if it gave the same final robot accuracy each time. The calibration had a repeatability of less than 0.04 mm for all axes.

Another source of error comes from segmentation inaccuracies. Contrary to CT images [19], in the case of MR images, this error is exacerbated by the less reliable quality of the signal. Indeed, in this prototype, the needle fiducials were smaller than in the previous LPR v2 prototype for space reasons. In the MRI images, this turned out to reduce their signal quality. In contrast, the frame fiducials that have five times the volume have a more accurate signal and are less subject to misalignment inaccuracies. This difference in signal quality affected the ability of the

fully automatic segmentation routine to consistently find a complete solution. To improve the segmentation accuracy in MRI, the needle fiducials would have to be enlarged to create a stronger signal.

The relatively long apnea needed during acquisition (28 s) limits patient selection. This length of time is required to obtain sufficient spatial resolution and volume acquisition to include and locate fiducials on the robot's frame and the needle gripper. We assume that, once a first acquisition has been made, the FOV could be reduced to focus on the needle gripper and the needle fiducial, to decrease the acquisition time and thus the length of apnea. We note that in CT acquisition is far faster. In the long term, breathing support and its influence on inner organ movements require study.

Finally, the robot's accuracy seems promising but supplementary studies need to be conducted to confirm these pre-clinical results.

Acknowledgements Sponsor: Grenoble Alpes University Hospital (Délégation à la Recherche Clinique et à l'Innovation). CIC-IT: This study was supported by the Clinical Research Center – Technological Innovation INSERM 1406 of Grenoble Alpes University Hospital. We thank Alison Foote (Ph.D. (Grenoble Alpes University Hospital) for critical editing.

Funding French National Research Agency (ANR)

Compliance with Ethical Standards

Conflict of interest The authors declare that they have no competing interest.

References

1. Wood B, Ramkaransingh J, Fojo T, et al. Percutaneous tumor ablation with radiofrequency. Cancer. 2002;94(2):443–51.
2. Walsh C, Sapkota B, Kalra M, et al. Smaller and deeper lesions increase the number of acquired scan series in computed tomography-guided lung biopsy. J Thorac Imaging. 2011;26:196–203.
3. Onik G, Cosman E, Wells T, et al. CT-guided aspirations for the body: comparison of hand guidance with stereotaxis. Radiology. 1988;166(2):389–94.
4. Arnolli M, Hanumara N, Franken M, et al. An overview of systems for CT- and MRI-guided percutaneous needle placement in the thorax and abdomen. Int J Med Robot. 2015;11(4):458–75.
5. Cleary K, Melzer A, Watson V, et al. Interventional robotic systems: applications and technology state of the art. Minim Invasive Ther Allied Technol. 2006;15(2):101–13.
6. Schell B, Eichler K, Mack MG, et al. Robot-assisted biopsies in a high-field MRI system—first clinical results. Rofo. 2012;184(1):42–7.
7. Stoianovici D, Cleary K, Patriciu A, et al. AcuBot: a robot for radiological interventions. IEEE Trans Robot Autom. 2003;19(5):927–30.
8. Cleary K, Watson V, Lindisch D, et al. Precision placement of instruments for minimally invasive procedures using a "needle driver" robot. Int J Med Robot. 2005;1(2):40–7.
9. Groetz S, Wilhelm K, Willinek W, et al. A new robotic assistance system for percutaneous CT-guided punctures: initial experience. Minim Invasive Ther Allied Technol. 2016;25(2):79–85.
10. Christoforou E, Seimenis I, Andreou E, et al. A novel, general-purpose, MR-compatible, manually actuated robotic manipulation system for minimally invasive interventions under direct MRI guidance. Int J Med Robot. 2014;10(1):22–34.
11. Melzer A, Gutmann B, Remmele T, et al. Innomotion for percutaneous image-guided interventions: principles and evaluation of this MR- and CT-compatible robotic system. IEEE Eng Med Biol Mag. 2008;27(3):66–73.
12. Maurin B, Bayle B, Piccin O, et al. A patient-mounted robotic platform for CT-scan guided procedures. IEEE Trans Biomed Eng. 2008;55(10):2417–25.
13. Walsh C, Hanumara N, Slocum A, et al. A patient-mounted, telerobotic tool for CT-guided percutaneous interventions. J Med Devices. 2008;2(1). https://doi.org/10.1115/1.2902854.
14. Wu FY, Torabi M, Yamada A, et al. An MRI coil-mounted multiprobe robotic positioner for cryoablation. Harvard Biodesign Lab. https://biodesign.seas.harvard.edu. Updated September 9, 2014.
15. Hungr N, Fouard C, Robert A, et al. Interventional radiology robot for CT and MRI guided percutaneous interventions. Med Image Comput Comput Assist Interv. 2011;14:137–44.
16. Hungr N, Bricault I, Cinquin P, et al. Design and validation of a CT and MRI guided robot for percutaneous needle procedures. IEEE Trans Robot. 2016;32(4):973–87.
17. Bricault I, Zemiti N, Jouniaux E, et al. Light puncture robot for CT and MRI interventions: designing a new robotic architecture to perform abdominal and thoracic punctures. IEEE Eng Med Biol Mag. 2008;27(3):42–50.
18. Taillant E, Avila-Vilchis J, Allegrini C, et al. CT and MR compatible Light Puncture Robot: architectural design and first experiments. In: Barillot C, Haynor D, Hellier P, editors. Medical image computing and computer-assisted intervention—MICCAI, proceedings, part II. Saint-Malo, France: Springer; 2004. p. 145–152.
19. Zemiti N, Bricault I, Fouard C, et al. LPR: a CT and MRI-compatible puncture robot to enhance accuracy and safety of image-guided interventions. IEEE/ASME Trans Mechatron. 2008;13(3):306–15.
20. Krieger A, Metzger G, Fichtinger G, et al. A hybrid method for 6-DOF tracking of MRI-compatible robotic interventional devices. In: Robotics Automation; 2006. p. 3844–3849.
21. Promayon E, Fouard C, Bailet M, et al. Using CamiTK for rapid prototyping of interactive computer assisted medical intervention applications. In: Conf Proc IEEE Eng Med Biol Soc; 2013. p. 4933–4936.